Comput Geosci (2015) 19:655–671
DOI 10.1007/s10596-014-9458-3

ORIGINAL PAPER

Implementation and evaluation of permeability-porosity and tortuosity-porosity relationships linked to mineral dissolution-precipitation

Mingliang Xie · K. Ulrich Mayer · Francis Claret · Peter Alt-Epping · Diederik Jacques · Carl Steefel · Christophe Chiaberge · Jiri Simunek

Received: 20 May 2014 / Accepted: 29 October 2014 / Published online: 20 November 2014

Abstract Changes of porosity, permeability, and tortuosity due to physical and geochemical processes are of vital importance for a variety of hydrogeological systems, including passive treatment facilities for contaminated groundwater, engineered barrier systems (EBS), and host rocks for high-level nuclear waste (HLW) repositories. Due to the nonlinear nature and chemical complexity of the problem, in most cases, it is impossible to verify reactive transport codes analytically, and code intercomparisons are the most suitable method to assess code capabilities and model performance. This paper summarizes model intercomparisons for six hypothetical scenarios with generally increasing geochemical or physical complexity using the reactive transport codes CrunchFlow, HP1, MIN3P, PFlotran, and TOUGHREACT. Benchmark problems include the enhancement of porosity and permeability through mineral dissolution, as well as near complete clogging due to localized mineral precipitation, leading to reduction of permeability and tortuosity. Processes considered in the benchmark simulations are advective-dispersive transport in saturated media, kinetically controlled mineral dissolution-precipitation, and aqueous complexation. Porosity changes are induced by mineral dissolution-precipitation reactions, and the Carman-Kozeny relationship is used to describe changes in permeability as a function of porosity. Archie's law is used to update the tortuosity and the pore diffusion coefficient as a function of porosity. Results demonstrate that, generally, good agreement is reached amongst the computer models despite significant differences in model formulations. Some differences are observed, in particular for the more complex scenarios involving clogging; however, these differences do not affect the interpretation of system behavior and evolution.

Keywords Permeability-porosity relationship · Tortuosity-porosity relationship · Mineral dissolution-precipitation · Benchmark · CrunchFlow · HP1 · MIN3P · PFlotran · TOUGHREACT

Electronic supplementary material The online version of this article (doi:10.1007/s10596-014-9458-3) contains supplementary material, which is available to authorized users.

M. Xie (✉) · K. U. Mayer
Department of Earth, Ocean and Atmospheric Sciences, The University of British Columbia, Vancouver, BC, Canada
e-mail: mxie@eos.ubc.ca

F. Claret · C. Chiaberge
BRGM, 45060 Orleans Cedex, France

P. Alt-Epping
Rock-Water Interaction Group, Institute of Geological Sciences, University of Bern, 3012 Bern, Switzerland

D. Jacques
Belgian Nuclear Research Centre SCK. CEN, B-2400 Mol, Belgium

C. Steefel
Lawrence Berkeley National Laboratory, Berkeley, CA 94720, USA

J. Simunek
University of California, Riverside, CA 92521, USA

1 Introduction

The simulation of permeability and tortuosity evolution due to porosity changes is of vital importance for the description of various hydrogeological processes, such as fluid circulation in geothermal systems [1], acid rock drainage (ARD) attenuation and treatment [2], well fouling due to oxide precipitation [3], aquifer storage and recovery (ASR)

[4], and the long-term geochemical evolution of host rock considered for high-level nuclear waste (HLW) repositories [5–7]. Porosity changes can be the result of many processes including mechanical deformation, swelling of clay minerals (e.g., montmorillonite), dissolution/precipitation, and thermal deformation. Mineral dissolution and precipitation reactions can also have a significant effect on porous medium porosity and in turn permeability and tortuosity.

Porosity changes in natural porous media occur normally very slowly, but in the long term can be of pivotal importance for the migration of fluids and solutes. If porosity increases are substantial, preferential fluid migration pathways may develop, accelerating solute transport. On the other hand, for significant porosity decreases, nearly complete clogging may occur, substantially inhibiting fluid and solute migration. Clogging in particular is associated with numerical challenges due to the development of very small water-rock ratios, or the complete disappearance of the aqueous phase. It is therefore useful to evaluate the capabilities and performance of reactive transport codes to simulate evolving porosity and permeability, both for conditions of porosity enhancement and reduction. It is also of interest to evaluate the effect of changing tortuosity on pore diffusion, in particular for clogging-dominated problems. Ideally, the verification of numerical models is conducted by comparing results to analytical solutions. For simulations involving porosity evolution, this is only possible for problems with a limited set of reactions and subject to simplifying assumptions [8–10]. However, considering the complex nature of realistic reactive transport problems, model verification by means of code intercomparisons through well-defined benchmarks is in many cases the only practical method [11].

This paper presents and analyzes the results of an intercomparison involving five reactive transport codes (i.e., CrunchFlow, HP1, MIN3P, PFlotran, and TOUGHREACT) used for the investigation of six hypothetical scenarios to evaluate formulations and implementations for permeability-porosity and tortuosity-porosity relationships. Transport and reaction processes considered include multicomponent aqueous complexation, kinetic surface-controlled reversible mineral dissolution and precipitation, advective and diffusive mass transport, and coupling of dissolution-precipitation-induced porosity change and fluid flow processes. The Carman-Kozeny relationship was used to describe changes in permeability, and the tortuosity and pore diffusion coefficients were updated based on Archie's law, both as a function of porosity.

2 Problem overview

Six benchmark levels with increasing complexity were investigated in this exercise (Table 1)—the first level (B1) considers mineral dissolution and associated permeability enhancement, the second level (B2) focuses on a precipitation-dominated (clogging) problem, and the third level (B3) extends the clogging problem of benchmark B2 by considering a significantly more complex geochemical system (e.g., inclusion of additional chemical components and minerals). Benchmarks B1–B3 have in common that advection is the only transport process considered. The fourth level (B4) is based on benchmark B3, but considers diffusive transport instead of advective transport to compare

Table 1 Overview of the benchmarks

Benchmark level	Description	Dimension	Processes	$t_{\text{Final}^{\#}}$ [years]
B1	Dissolution only		Advection, kinetic dissolution	500
B2	Clogging in a simple geochemical system		Advection, kinetic dissolution/precipitation	1000
B3		1D homogeneous (2 m in length)	Advection, kinetic dissolution/precipitation, redox reactions	300
B4			Diffusion, no advection, kinetic dissolution/precipitation, redox reactions	3000
B5	Clogging in a complex geochemical system		Advection, diffusion, kinetic dissolution/precipitation, redox reactions	300
B6		2D heterogeneous (3 m in length and 2 m in height)	Advection, diffusion, kinetic dissolution/ precipitation, redox reactions	300

[#]-Final simulation time

the codes under purely diffusive mass transfer conditions. The fifth level (B5) combines benchmarks B3 and B4 and includes both diffusive and advective transport. Benchmarks B1–B5 were carried out for 1D flow and transport systems with initially homogeneous medium properties. Benchmark B6 further extends B5 into a 2D heterogeneous problem with a randomly distributed hydraulic conductivity field.

Benchmark B1 considers the infiltration of a sulfuric acid solution into a rock matrix containing calcite in an otherwise nonreactive (inert) rock matrix. The only mineral phase considered is calcite; four components are included (H^+, Ca^{2+}, CO_3^{2-}, and SO_4^{2-}), leading to the formulation of 10 aqueous complexes. Benchmark B2 also considers the infiltration of a sulfuric acid solution into a calcite-containing rock matrix. In addition to the primary mineral phase calcite, gypsum is considered as a secondary phase. The inflow solution contains a much higher SO_4^{2-} concentration. Benchmark B3 is based on B2 by adding Fe(II), Fe(III), K, Al, Na, and O_2(aq), thus increasing the number of aqueous components (10), secondary aqueous species (40) and mineral phases (6). Benchmarks B4 to B6 use the same reaction network as benchmark B3. For benchmarks B4 to B6, the chemical composition of the solution at the inflow boundary and the pore water in the domain, and the mineral composition of the domain also remain the same as those in benchmark B3.

All simulations were conducted under standard pressure and temperature (25 °C) and fully saturated conditions. The geochemical database was derived from the database of MINTEQA2 ([12], see Supporting Information).

This set of benchmarks was solved by five different reactive transport codes, namely CrunchFlow [13], HP1 [14, 15] (restricted to B1–B5, because it is a 1D transport code), MIN3P [16, 17], PFlotran [18], and TOUGHREACT [19–21]. An overview on the formulations and capabilities of the individual codes is given in [13].

3 Theoretical background

The generalized governing equations for multicomponent reactive transport are provided in [13] and are therefore not repeated here. This section focuses on the formulations used to describe permeability-porosity and tortuosity-porosity relationships, which are central to this benchmark. In addition, the formulations for mineral dissolution-precipitation reactions and activity corrections are provided, considering that these relationships strongly affect the results of the benchmarks.

3.1 Porosity, permeability, and tortuosity

The porosity change in each grid cell is calculated by summation over the volume fraction (φ) changes of the minerals that occurred between the new time step ($t + \Delta t$) and that at the previous time step (t). Assuming that porosity changes are occurring slowly, porosity (ϕ) in each cell is explicitly updated after completion of each time step:

$$\phi^{t+\Delta t} = \phi^t - \sum_{i=1}^{N_m} (\varphi_i^{t+\Delta t} - \varphi_i^t) \tag{1}$$

where N_m defines the number of the minerals. The hydraulic conductivity is also updated at the end of each time step according to the Carman-Kozeny relationship [22]:

$$K^{t+\Delta t} = \left[\frac{(\phi^{t+\Delta t})^3}{\left[1-(\phi^{t+\Delta t})\right]^2}\right]\left[\frac{(1-\phi^t)^2}{(\phi^t)^3}\right] K^t \tag{2}$$

Archie's law is used to calculate the tortuosity τ as a function of porosity at the new time level:

$$\tau^{t+\Delta t} = \left[\phi^{t+\Delta t}\right]^{\alpha} \tag{3}$$

with the exponent $\alpha = 1/3$, consistent with the formulation by Millington and Quirk [23]. The pore diffusion coefficient at the new time level ($D_p^{t+\Delta t}$) is calculated as

$$D_p^{t+\Delta t} = \tau^{t+\Delta t} D_0 \tag{4}$$

where D_0 is the free phase diffusion coefficient in water (assumed to be identical for all species). The effective diffusion coefficient D_e is calculated as

$$D_e^{t+\Delta t} = \phi^{t+\Delta t}\tau^{t+\Delta t} D_0 = \phi^{t+\Delta t} D_p^{t+\Delta t} \tag{5}$$

3.2 Mineral dissolution-precipitation reactions

Mineral dissolution-precipitation reactions are described as kinetic surface-controlled reactions based on the rate expression:

$$R_i^m = -k_i^m \left[1 - \left(\frac{\mathrm{IAP}_i^m}{K_i^m}\right)\right] \tag{6}$$

where R_i^m is the reaction rate, IAP_i^m is the ion activity product, K_i^m is the equilibrium constant, and k_i^m is the effective rate constant. The rate constants k_i^m of primary minerals vary as a function of mineral abundance at each time step. For primary mineral phases, a two-third power relationship of the form

$$k_i^{m,t} = -k_i^{m,0}\left(\frac{\varphi_i^t}{\varphi_i^0}\right)^{2/3} \tag{7}$$

is used to update the effective rate constant [24]. In this relationship, $k_i^{m,t}$ and φ_i^t define the effective rate constant and mineral volume fraction at time t, respectively; while $k_i^{m,0}$ and φ_i^0 define the initial rate constant and mineral volume fraction, respectively. The rate coefficients for secondary minerals are assumed to remain constant.

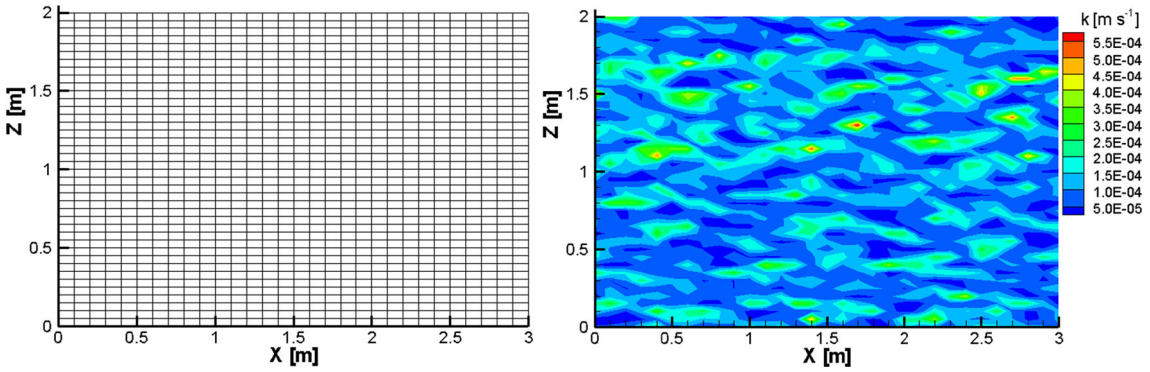

Fig. 1 2D geometry (left) and initial hydraulic conductivity distribution (in [m s^{-1}]) (right)

3.3 Activity corrections

Activity coefficients γ_i^d for all charged dissolved species A_i^d, where A_i^d can be either a component as species in solution or an aqueous complex, are calculated based on the modified Debye-Hückel equation if ion-specific parameters are available [12, 25]:

$$\log \gamma_i^d = \frac{-A_d Z_i^2 \sqrt{I}}{1 + B_d a_i \sqrt{I}} + b_i I \tag{8}$$

where I is the ionic strength, Z_i is the charge of the i^{th}ion, A_d and B_d are constants, a_i and b_i are ion-specific parameters. If a_i is available, but not b_i, Eq. 8 is used with $b_i = 0$. When a_i is not provided, the Davies equation is used as an approximation [12]:

$$\log \gamma_i^d = -A_d Z_i^2 \left[\frac{\sqrt{I}}{1 + \sqrt{I}} - 0.24 I \right] \tag{9}$$

Activity correction for neutral species excluding water is calculated as described by Allison et al. [12]:

$$\log \gamma_i^d = 0.1 I \tag{10}$$

The activity correction for water is defined by [12]:

$$\gamma_{H_2 0} = 1 - 0.017 \sum_{i=1}^{N_d} C_i^d \tag{11}$$

where C_i^d are the concentrations of the dissolved charged species and N_d defines the number of the dissolved charged species [12].

3.4 Numerical considerations

Benchmark levels B1–B3 do neither consider diffusion, nor dispersion, in order to allow for a better evaluation of numerical dispersion and operator-splitting errors as a function of different model formulations. Because significant spatial differences develop for porosity, hydraulic conductivity, and tortuosity, the spatial weighting of these parameters is important. Harmonic averaging of all flow and transport parameters (i.e., hydraulic conductivity and tortuosity) were adopted as the recommended default option for the simulations. For spatial weighting of the advection terms, upstream weighting was used; implicit time weighting was used for time integration.

Marty et al. [26] reported that spatial discretization intervals can have a substantial effect on the simulated clogging position, which could impact the model intercomparison. To avoid this issue, all codes used the same spatial discretization for each of the benchmarks B1–B6.

Similar to spatial discretization, it would be ideal to use the same temporal discretization amongst all codes for model intercomparison. However, phase disappearance of minerals and near complete clogging events often lead to convergence problems, which can be effectively addressed by automatic adjustment of the time steps. Under these

Table 2 Reaction stoichiometries and solubility constants for minerals

Mineral	Reaction	$\log K_{25}$
Calcite	$Ca^{2+} + CO_3^{2-} \leftrightarrow CaCO_3$	8.4750
Gypsum	$Ca^{2+} + SO_4^{2-} + 2H_2O \leftrightarrow CaSO_4{:}2H_2O$	4.5800
Ferrihydrite	$Fe^{3+} + 3H_2O \leftrightarrow Fe(OH)_3 + 3H^+$	-4.8910
Jarosite	$K^+ + 3Fe^{3+} + 2SO_4^{2-} + 6H_2O \leftrightarrow KFe_3(SO_4)_2(OH)_6 + 6H^+$	9.2100
Gibbsite	$Al^{3+} + 3H_2O \leftrightarrow Al(OH)_3 + 3H^+$	-8.1100
Siderite	$Fe^{2+} + CO_3^{2-} \leftrightarrow FeCO_3$	10.4500

Table 3 Physical and kinetic mineral parameters

Mineral	$k_i^{m,0}$ [m^2 mineral L^{-1} bulk]	Density [g cm^{-3}]	Mol. weight [g mol^{-1}]	Molar volume [cm^3 mol^{-1}]	Update type
Calcite	5×10^{-8}	2.71	100.09	36.93	Two third
Gypsum	5×10^{-8}	2.32	172.17	74.21	Constant
Ferrihydrite	5×10^{-9}	4.37	104.87	23.99	Constant
Jarosite	5×10^{-9}	3.20	494.81	154.63	Constant
Gibbsite	5×10^{-10}	2.35	78.00	33.19	Two third
Siderite	5×10^{-9}	3.96	115.86	29.26	Two third

circumstances, differences in model formulation make it difficult to use the same temporal discretization for all codes. To evaluate the effect of adaptive time stepping or constant time stepping for a range of time increments, a series of simulations were performed with the MIN3P code. It was found that the time increment size had an insignificant effect on the clogging position and outflow response (results not shown). It was therefore deemed adequate to let the various participants choose time increments that are most appropriate for the corresponding code and model formulation on numerical consideration.

A performance and efficiency comparison was not a goal of the exercise. Information on time stepping and Newton iteration count is therefore not provided.

4 Benchmark definition

4.1 Dimensions and spatial discretization

The 2-m-long 1D domain for benchmarks B1–B5 was discretized using a discretization interval of $\Delta x = 0.025$ m, corresponding to 80 cells for uniform discretization, or 81 cells with half cells on the boundaries. The 2D domain (3 m in length and 2 m in height) for benchmark B6 was discretized into $31 \times 41 = 1271$ cells (Fig. 1).

Table 4 Initial and boundary geochemical compositions in aqueous phase (B1)

Primary components	Unit	Initial condition	Boundary condition
pH	–	9.38	3.0
Ca^{2+}	mol l^{-1} H_2O	1.57×10^{-4}	1.00×10^{-4}
CO_3^{2-}	mol l^{-1} H_2O	2.57×10^{-4}	1.0×10^{-2}
SO_4^{2-}	mol l^{-1} H_2O	1.00×10^{-10}	6.46×10^{-4}

4.2 Physical properties

For the 1D problems B1 to B5, the porous medium is initially homogeneous with an initial porosity of 0.35 and an initial hydraulic conductivity of 1.16×10^{-4} m s^{-1} (10 m day^{-1}). An average free phase diffusion coefficient of 1.0×10^{-9} m^{-2} s^{-1} for all aqueous species is considered for benchmarks B4–B6. For problems including advection, dispersion is neglected to minimize the complexity of the problem and facilitate a focused comparison of the different codes. In addition, dispersion becomes insignificant when clogging occurs, due to reduced flow velocities and the localized nature of pore clogging due to mineral precipitation. For the 2D problem B6, advective and diffusive transport is considered in a similar fashion to B5; however, the porous medium is characterized by a heterogeneous initial hydraulic conductivity field (Fig. 1).

4.3 Boundary conditions for flow

Benchmarks B1–B4 considered constant hydraulic heads at the inflow (0.007 m) and outflow (0.0 m) boundaries. For benchmark B4, no-flow conditions are enforced by setting equal hydraulic heads at the inflow and outflow boundaries. For benchmark B6, the hydraulic head at the inflow boundary was set at 0.0105 m to maintain the same hydraulic gradient as with all other benchmarks (except B4).

4.4 Mineralogical and chemical parameters

4.4.1 Aqueous components and speciation reactions

The components for benchmarks B1 and B2 are H^+, CO_3^{2-}, Ca^{2+}, SO_4^{2-}, and Na^+. An enhanced set of components is used for benchmarks B3–B6 (H^+, CO_3^{2-}, Ca^{2+}, SO_4^{2-}, Fe^{3+}, Fe^{2+}, Al^{3+}, K^+, O_2(aq), and Na^+). Relevant aqueous complexation reactions and activity model parameters are tabulated in the Supporting Information.

Table 5 Initial mineral composition and saturation index (SI) in the initial and boundary solutions (B2)

Mineral	Initial volume fraction [$m^3\ m^{-3}$]	SI (IC solution)	SI (BC solution)
Calcite	0.3	0.0	−9.1
Gypsum	0.0	−3.1	−1.9

Table 6 Initial and boundary geochemical compositions in aqueous phase (B2)

Primary components	Unit	Initial condition (IC)	Boundary condition (BC)
pH	pH	9.33	3.0
Ca^{2+}	mol l^{-1} H_2O	1.70×10^{-4}	1.0×10^{-4}
CO_3^{2-}	mol l^{-1} H_2O	2.70×10^{-4}	1.0×10^{-2}
SO_4^{2-}	mol l^{-1} H_2O	1.70×10^{-4}	0.2
Na^{+}	mol l^{-1} H_2O	3.20×10^{-4}	3.96×10^{-1}

Table 7 Initial mineral composition and saturation index (SI) in the initial and boundary solutions (B3–B6)

Mineral	Initial volume fraction [$m^3\ m^{-3}$]	SI (IC solution)	SI (BC solution)
Calcite	0.22	0.00	−8.93
Gypsum	0.00	−2.78	−2.02
Ferrihydrite	0.00	0.00	−0.07
Jarosite	0.00	−12.97	6.66
Gibbsite	0.05	0.00	−2.94
Siderite	0.05	0.00	−10.89

Table 8 Initial and boundary geochemical compositions in aqueous phase (B3–B6)

Primary components	Unit	Initial condition (IC)	Boundary condition (BC)
pH	–	8.01	3.0
pe	–	−0.67	17.53
Ca^{2+}	mol l^{-1} H_2O	4.71×10^{-4}	1.00×10^{-4}
CO_3^{2-}	mol l^{-1} H_2O	2.19×10^{-3}	1.00×10^{-2}
SO_4^{2-}	mol l^{-1} H_2O	1.70×10^{-4}	1.00×10^{-1}
Na^{+}	mol l^{-1} H_2O	1.54×10^{-3}	9.09×10^{-2}
Al^{3+}	mol l^{-1} H_2O	2.81×10^{-7}	1.43×10^{-2}
K^{+}	mol l^{-1} H_2O	1.00×10^{-5}	7.67×10^{-5}
Fe^{2+}	mol l^{-1} H_2O	6.59×10^{-6}	1.14×10^{-8}
Fe^{3+}	mol l^{-1} H_2O	2.53×10^{-8}	2.23×10^{-2}

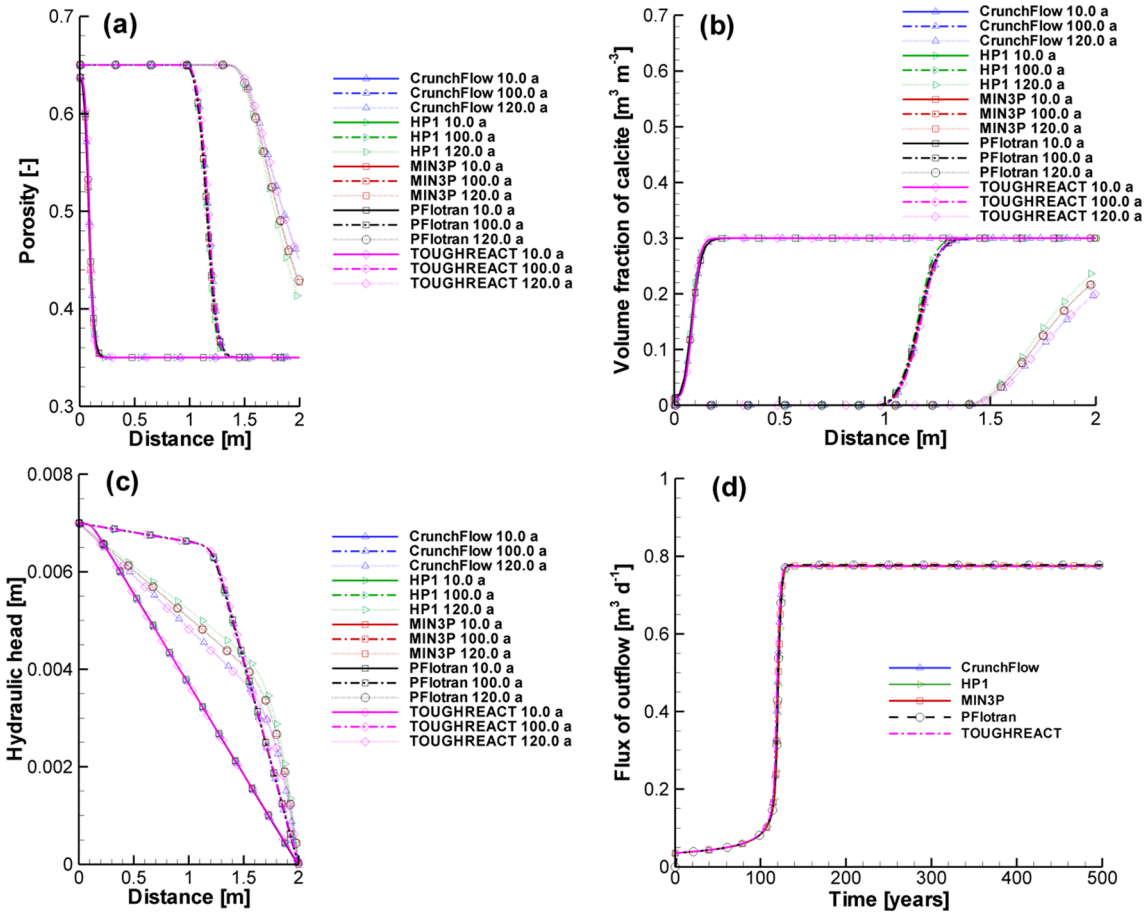

Fig. 2 Profiles of porosity (a), volume fraction of calcite (b), and hydraulic head (c) at 10, 100, and 120 years, and flux time curve (d) from the outflow boundary simulated by CrunchFlow, HP1, MIN3P, PFlotran, and TOUGHREACT

4.4.2 Minerals

Mineral phases and their parameters are listed in Tables 2 and 3. Benchmarks B1 and B2 use a subset of these mineral phases. All minerals are treated as kinetic surface-controlled dissolution/precipitation reactions. The only exception is jarosite, which was treated as an equilibrium reaction by HP1 owing to numerical difficulties. The initial rate constants ($k_i^{m,0}$) are shown in Table 3.

4.4.3 Initial and boundary conditions for reactive transport

Benchmark B1 The only mineral phase considered is calcite at a volume fraction of 0.30 $m^3\ m^{-3}$, the remaining fraction of the solid phase is assumed inert. The solution domain is initially occupied by an alkaline solution in equilibrium with calcite. The infiltrating water is acidic with a pH of 3 and is undersaturated with respect to calcite (Table 4). A third type boundary condition (specified mass flux) is used at the inflow boundary and a free exit boundary is used at the outflow.

Benchmark B2 The mineral phases considered in the system are calcite and gypsum. The domain initially includes only calcite with a volume fraction of 0.30 $m^3\ m^{-3}$ (Table 5). Resident pore water is in equilibrium with calcite and undersaturated with respect to gypsum (Table 6).

With the infiltration of a sulfuric acid solution (pH = 3) containing CO_3^{2-}, Ca^{2+}, SO_4^{2-}, and Na^+, calcite dissolves and gypsum precipitates, followed by gypsum re-dissolution near the inflow boundary. The initial and boundary geochemical compositions for the aqueous phases are listed in Table 6. Boundary conditions are set as in B1.

Benchmarks B3–B6 The domain initially contains calcite with a volume fraction of 0.22 $m^3\ m^{-3}$, as well as gibbsite (0.05 $m^3\ m^{-3}$) and siderite (0.05 $m^3\ m^{-3}$) (Table 7). The initial and boundary total component concentrations in the aqueous phases are listed in Table 8. The incoming solution is acidic and undersaturated with respect to all minerals, except jarosite. This boundary condition was specified to induce jarosite precipitation near the inflow. The background solution is slightly alkaline and is in equilibrium

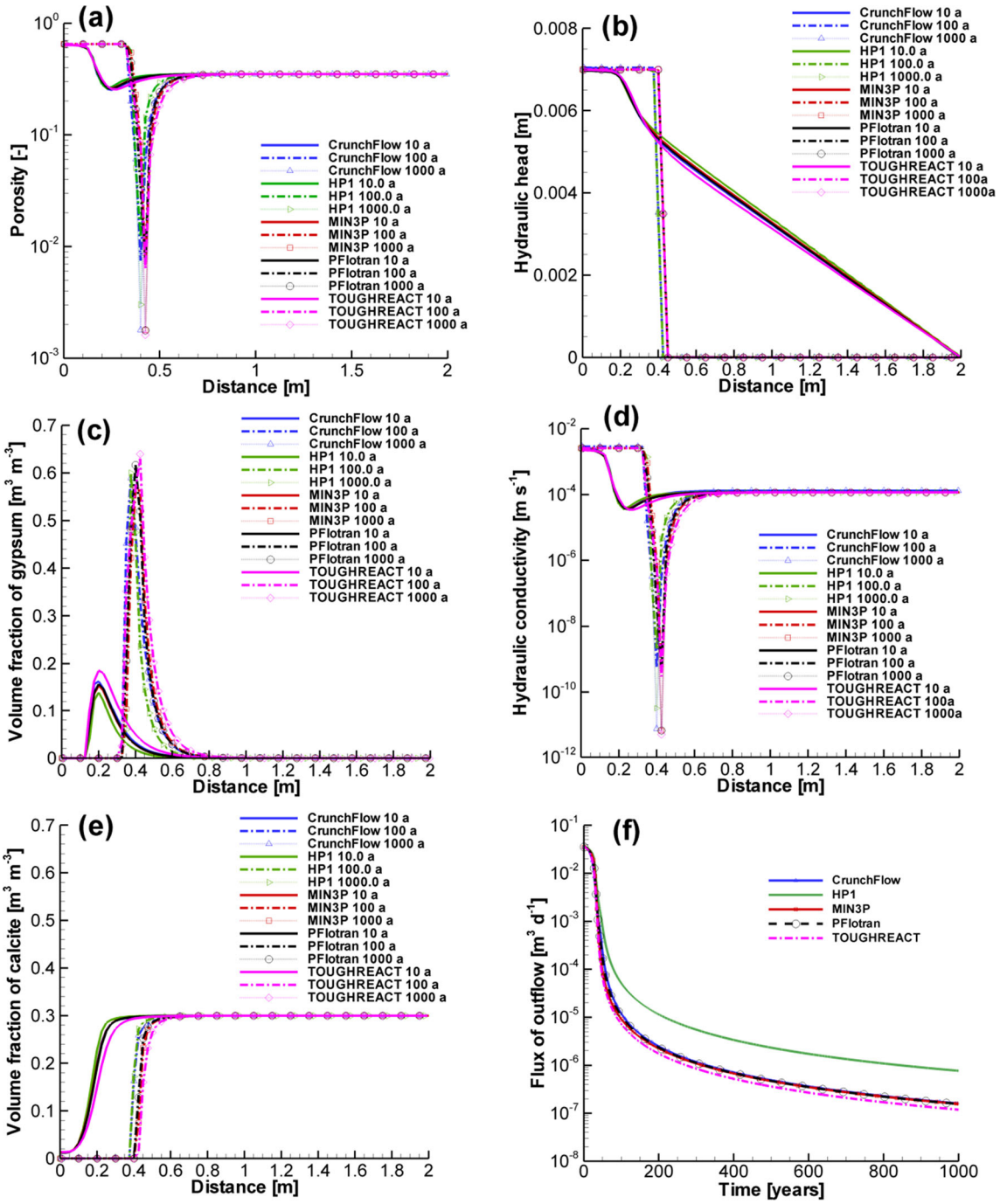

Fig. 3 Profiles (B2) of porosity (a), volume fraction of gypsum (c) and calcite (e), hydraulic head (b), hydraulic conductivity (d) at 10, 100, and 120 years, and flux from the outflow boundary (f) simulated by CrunchFlow, HP1, MIN3P, PFlotran, and TOUGHREACT

with calcite, siderite, gibbsite, and ferrihydrite. The initial volume fraction of calcite (0.22 $m^3\ m^{-3}$) is lower than that in B2. The lower calcite content limits secondary gypsum formation, which is offset by additional precipitation of ferrihydrite, siderite, gibbsite, and jarosite. This approach is taken to provide a suitable benchmark that evaluates system evolution under near clogging conditions. Boundary conditions are set as in B1 and B2, with the exception of benchmark B4 which uses first-type (Dirichlet) boundary conditions at the inflow and outflow ends of the column.

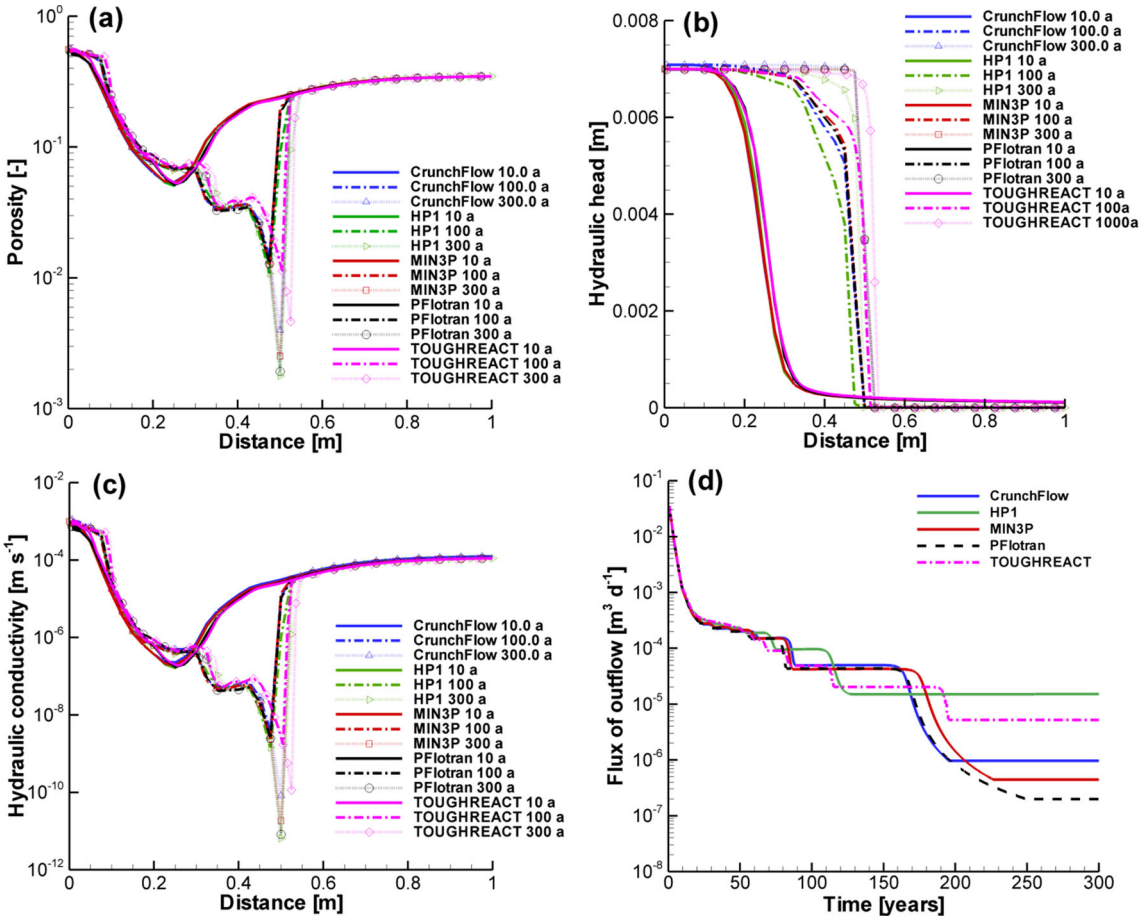

Fig. 4 Comparison of profiles (B3) of porosity, hydraulic head, and hydraulic conductivity at 10, 100 and 300 years, and outflux time curve from the outflow boundary simulated by CrunchFlow, HP1, MIN3P, PFlotran, and TOUGHREACT

5 Results

Simulated results by all codes are discussed in the following subsections. Reference model results produced by MIN3P are also provided in tabular format in the Supporting Information.

5.1 B1—porosity and permeability change due to dissolution

Simulation results for benchmark B1 show the gradual dissolution of calcite along an initially narrow dissolution front, which widens as permeability and flow velocities increase (Fig. 2). Although porosity and permeability increase substantially near the inflow end already at early time, total flow rate increases are relatively moderate during the first 100 years. However, a rapid increase in flow rate is predicted, once calcite depletion approaches the outflow end of the simulation domain. All profiles of porosity, permeability, and hydraulic head at 10 and 100 years calculated by the five codes are nearly identical, demonstrating very good agreement between the models, despite different transport schemes and coupling methods. Slight differences exist for results at 120 years. This time correlates with the breakthrough of the dissolution front and is naturally most sensitive to deviations. The time curves of the flux at the outflow boundary are identical for all codes up to 120 years.

5.2 B2—clogging due to dissolution/precipitation (simple reaction network)

Simulation results show that the intrusion of the sulfuric acid solution causes the dissolution of calcite and formation of gypsum (Fig. 3). Although gypsum re-dissolves near the inflow, a narrow region of gypsum accumulation causes clogging of the flow path. The zone of gypsum accumulation is already visible after 10 years; however, significant porosity remains at this time. After 100 years, clogging is nearly complete and flow rates are greatly reduced, resulting in negligible clogging front migration over the remaining

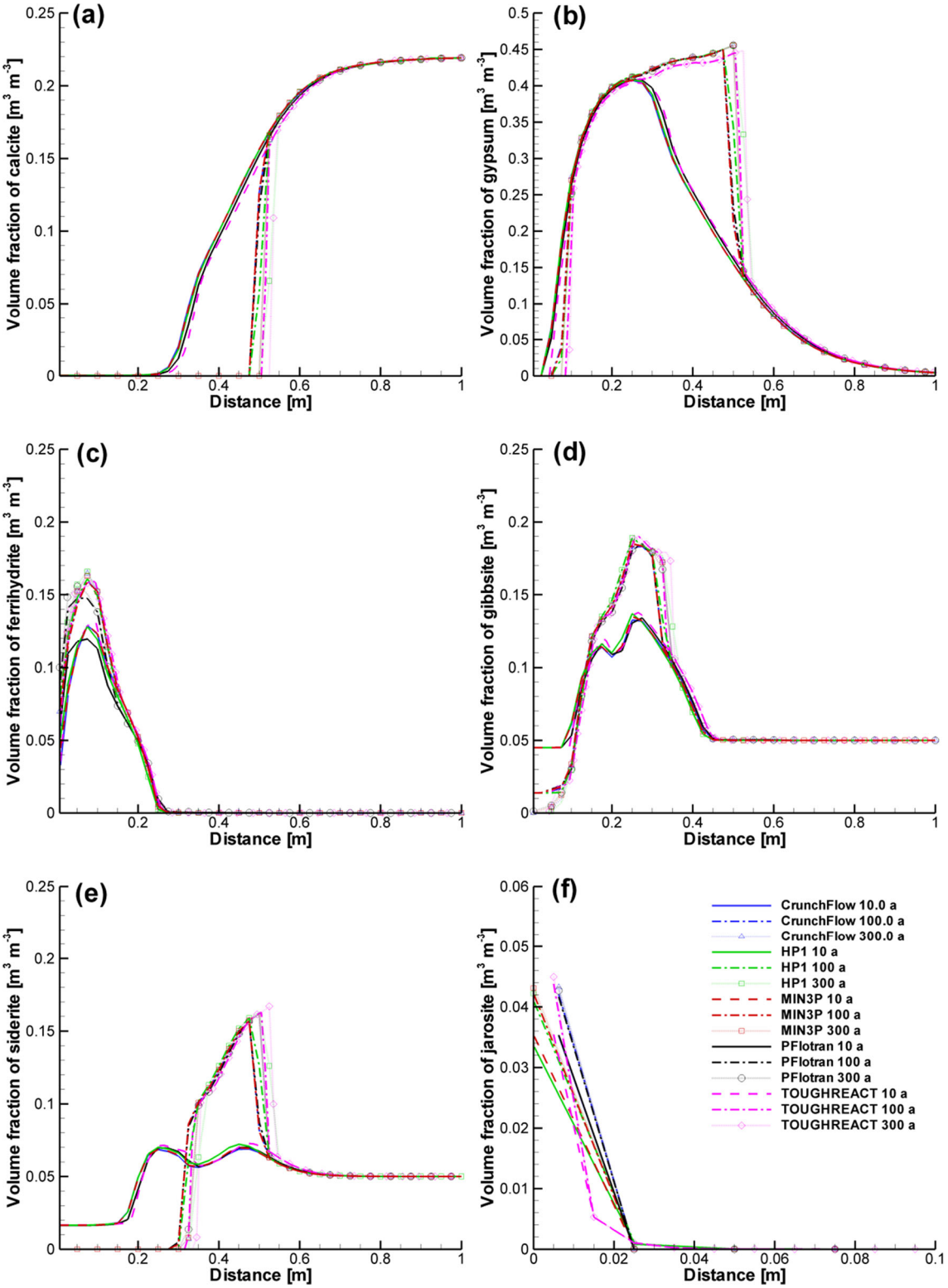

Fig. 5 Comparison of volume fraction profiles (B3) of calcite (a), gypsum (b), ferrihydrite (c), gibbsite (d), siderite (e), and jarosite (f) at 10, 100, and 300 years simulated by CrunchFlow, HP1, MIN3P, PFlotran, and TOUGHREACT

900 years. Simulated results show good agreement between all codes. The maximum volume fraction of gypsum reaches 62.6 % and results in the reduction of porosity with a minimum value of 0.0016 after 1000 years at $x = 0.425$ m (MIN3P, PFlotran, and TOUGHREACT), at $x = 0.40$ m with a minimum porosity of 0.003 (HP1) and at $x = 0.40$ m

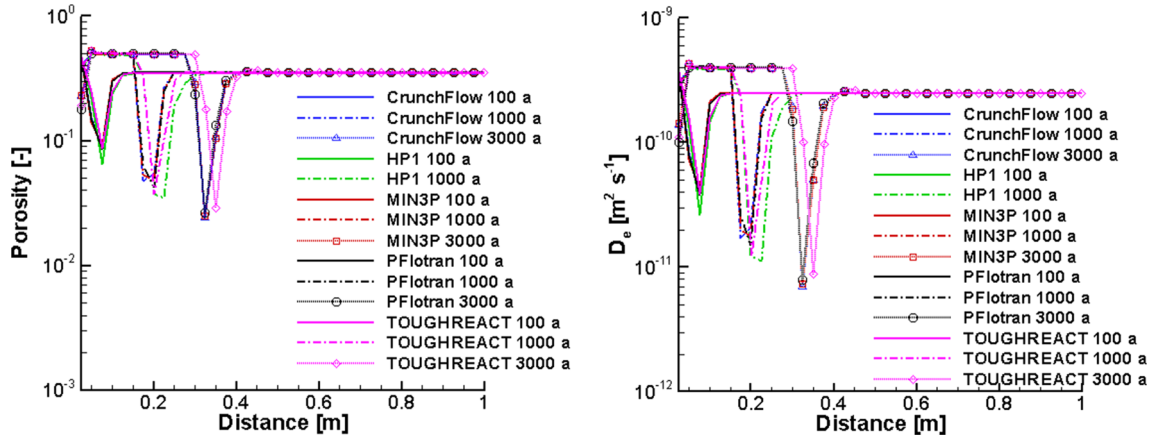

Fig. 6 Comparison of profiles (B4) of porosity (left) and effective diffusion coefficient (D_e) (right) at 100, 1000 and 3000 years simulated by CrunchFlow, MIN3P, PFlotran, TOUGHREACT, and HP1 (at 100 and 1000 years)

with a minimum porosity of 0.0018 (CrunchFlow). The simulated profiles of the hydraulic head show a sharp decline at the clogging point. The calculated flux at the outflow boundary decreased rapidly within the first 100 years and more gradually after 500 years (Fig. 3), showing good agreement amongst all codes with small deviations by HP1 owing to the higher minimum value of porosity by HP1.

5.3 B3—clogging due to dissolution/precipitation (complex reaction network—advection)

Simulated results (Figs. 4 and 5) show that with the infiltration of the acidic solution, calcite dissolves, while other minerals like gypsum, siderite, gibbsite, and ferrihydrite dissolve or precipitate depending on the time and location, thus forming various porosity modifications along the flow path at different time levels (Fig. 5). Jarosite precipitates near the inflow; consequently, the porosity decreases near the infiltration boundary. However, the major porosity reduction occurs due to the dissolution of calcite and precipitation of gypsum, similar to benchmark level B2. At 10 years, the minimum porosity reduces from the initial value of 0.35 to 0.05 at 0.25 m, showing a tendency for clogging (Fig. 4). The "clogging point" develops and moves further downstream to 0.45 m at 100 years. Beyond 100 years, however, the clogging point moves more slowly (Fig. 4, top left), as clogging is nearly complete and water and solute fluxes are greatly reduced. At 300 years, the minimum porosity reached is 0.0044 (CrunchFlow), 0.0020 (HP1), 0.0028 (MIN3P), 0.0022 (PFlotran), and 0.0048 (TOUGHREACT).

Overall, the model results compare well for all five codes; all models are in good agreement with respect to the prediction of the mineral distribution and clogging location. However, there appears to be significant differences in terms of outflux at the end of the simulation (ranging over approximately 2 orders of magnitude). On the other hand, this apparent mismatch has to be put into perspective. Comparing the residual outflux to the initial outflux at $T = 0$ demonstrates that all models predict a reduction of flux by greater than 99.9 %, which again points to a very good agreement in terms of predicting both hydrogeologic and geochemical evolution. Reasons for residual differences are likely due to the high sensitivity of fluxes to minor variations in porosity, which in turn is affected by the formation and dissolution of multiple mineral phases. These results highlight the challenges that numerical models encounter due to clogging and phase disappearance.

5.4 B4—clogging due to dissolution/precipitation (complex reactions network—diffusion)

Diffusive transport results in a similar geochemical evolution as simulated in the advective case (B3), but with mineral dissolution/precipitation fronts that are moving more slowly. Consequently, the kinetic limitations have a smaller effect on the results, which can be seen by the comparison of the profiles for jarosite. Jarosite was treated as a kinetically controlled mineral dissolution/precipitation reaction by all codes except HP1. The simulated results at 100 and 1000 years by HP1 agree better to those by CrunchFlow, MIN3P and PFlotran in comparison to benchmark B3 (compare Figs. 7 and 5). Figure 6 (left) shows a region of reduced porosity, leading to reductions in tortuosity and effective diffusion coefficients (D_e) (Fig. 6 right). The point with minimal porosity is located at 0.325 m after 3000 years. Simulated geochemical and hydrogeological evolution (Fig. 6) as well as mineralogical composition (Fig. 7) by all participating codes showed good agreement. Generally, the simulated profiles of mineral volume fractions by MIN3P CrunchFlow and PFlotran agree very well with slight difference for ferrihydrite and jarosite. Simulated mineral composition profiles by TOUGHREACT and

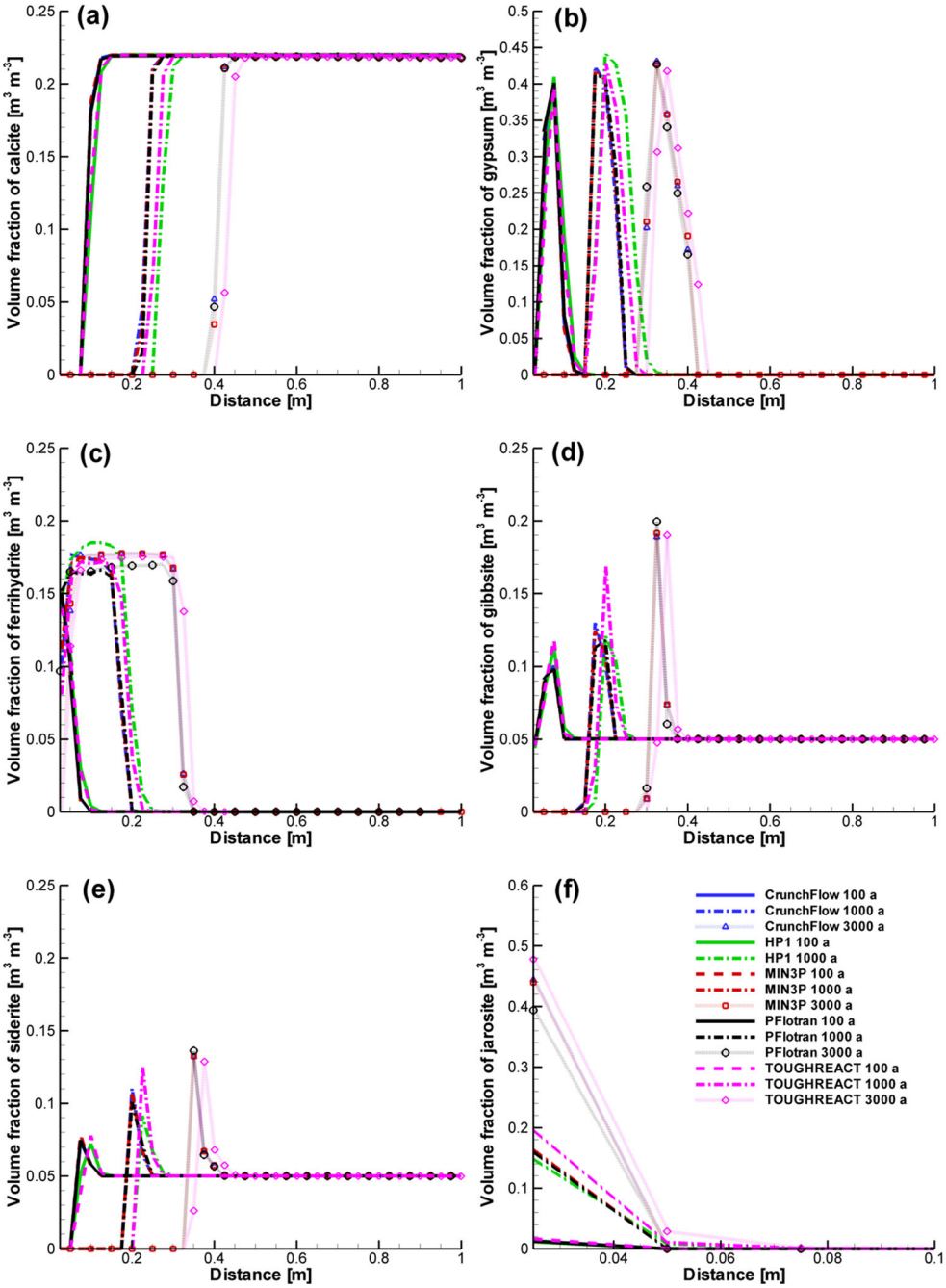

Fig. 7 Comparison of mineral volume fraction profiles (B4) of calcite (**a**), gypsum (**b**), ferrihydrite (**c**), gibbsite (**d**), siderite (**e**) and jarosite (**f**) at 100, 1000 and 3000 years simulated by CrunchFlow, MIN3P, PFlotran and TOUGHREACT, and HP1 (for 100 and 1000 years)

HP1 showed slightly faster moving fronts for all minerals, but visual agreement amongst all codes can be considered as good.

5.5 B5—clogging due to dissolution/precipitation (complex chemical reactions—advection and diffusion)

Overall, the predicted geochemical and hydrogeological evolution (Fig. 8), as well as mineralogical composition (Fig. 9) are in agreement for all participating codes. The clogging positions of all simulations are at 0.5 m, which closely coincides with the position determined in benchmark B3. This indicates that the clogging position is controlled by the advective mass transport for the benchmark set considered here. The distributions of most minerals in B5 resemble those of B3 with slight differences in the location of the moving fronts except jarosite simulated by HP1. This can be explained because jarosite precipitation is treated as an equilibrium phase instead of kinetic precipitation, as specified in the benchmark

In contrast to benchmark B3, larger differences can be seen for outflux and minimum porosity (Fig. 8). The

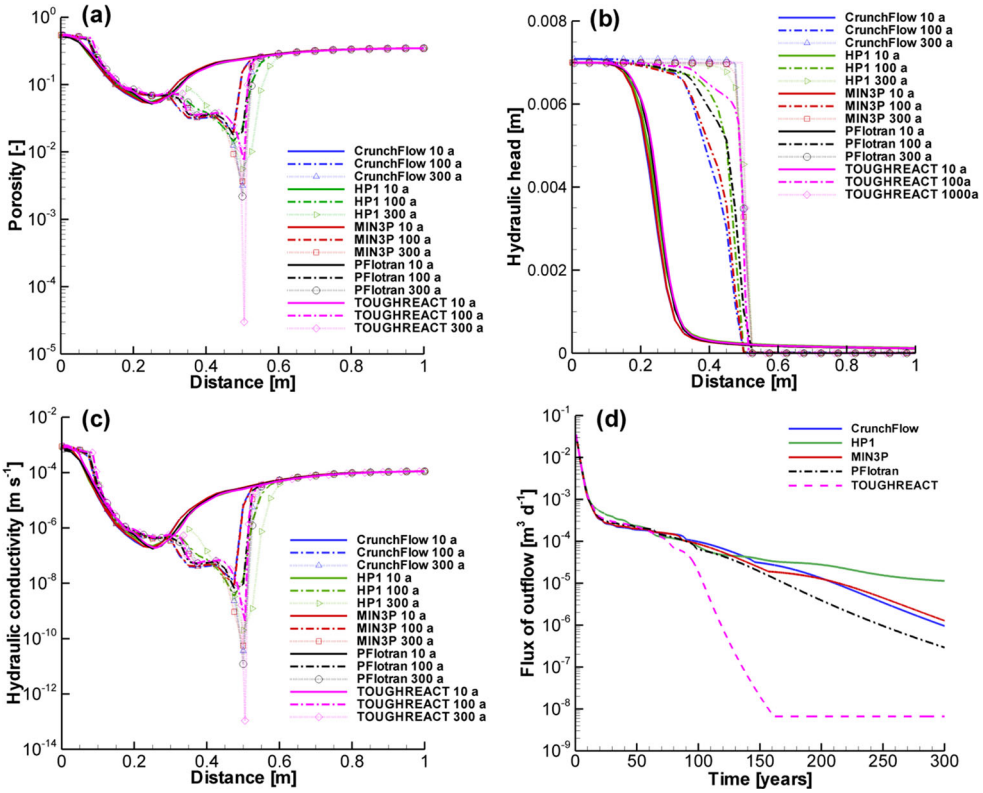

Fig. 8 Comparison of profiles (B5) of porosity (**a**), hydraulic head (**b**) and hydraulic conductivity (**c**) at 10, 100 and 300 years, and outflux time curve from the outflow boundary (**d**) simulated by CrunchFlow, HP1, MIN3P, PFlotran, and TOUGHREACT

simulated fluxes are fairly close within the first 90 years. At later time, simulated fluxes by MIN3P, HP1, PFlotran and CrunchFlow decrease gradually (Fig. 8), while TOUGHREACT results suggest a substantial reduction of permeability that remains constant after about 160 years. Although all fluxes are small in relation to the initial flux through the system, the final predicted outfluxes vary by more than 4 orders of magnitude. The predicted outfluxes by MIN3P, PFlotran and CrunchFlow vary by less than 2 orders of magnitude. These differences suggest that the numerical formulation of diffusion processes plays a key role for simulating porosity evolution, despite the fact that the problem is initially advection-dominated. In comparison to B3, reduction of fluxes occurs smoothly (compare Figs. 4 and 8). This indicates that diffusion tends to slow down clogging in this scenario but leads to substantial reduction of the minimum porosity and flux in the long term.

5.6 B6—clogging due to dissolution/precipitation in heterogeneous media

Simulated porosities for the 2D heterogeneous scenario are depicted in Fig. 10 for two selected observation points P1 ($x = 0.1$ m, $z = 1.0$ m) and P2 ($x = 0.5$ m, $z = 1.0$ m) for MIN3P, CrunchFlow, TOUGHREACT and PFlotran. At P2 all simulated results of porosity evolution show good agreement—with a rapid decrease during the first 20 years and a slight increase thereafter (Fig. 10). At P1, the simulated porosity show the same trend for the first 10 years, but the minimum porosity values differ substantially. At later time, the porosity increases again, gently according to MIN3P and CrunchFlow results, but more strongly according to the results obtained with PFlotran and TOUGHREACT.

The simulated flux curves by MIN3P, CrunchFlow, TOUGHREACT and PFlotran show a gradually decreasing trend with good agreement (Fig. 11). The flux declined very rapidly over the first 10 years, during which all simulated results are almost identical. At later times, the flux continues to decrease but at a reduced rate. These results seem to contradict the simulated porosity evolution at the observation points, which showed substantial differences at P1. However, these results also indicate that the overall permeability evolution is reproduced in a similar fashion by all codes, and that differences are local.

This observation is confirmed further by examining simulated 2D porosity distributions at 300 years. Results obtained with the different codes showed very similar pattern illustrating the effect of heterogeneity on clogging (Fig. 12). The low porosity zones (in blue), distributed between $x = 0.4$ and 0.7 m, tend to form a continuous low permeability belt, which prevents flow through the domain.

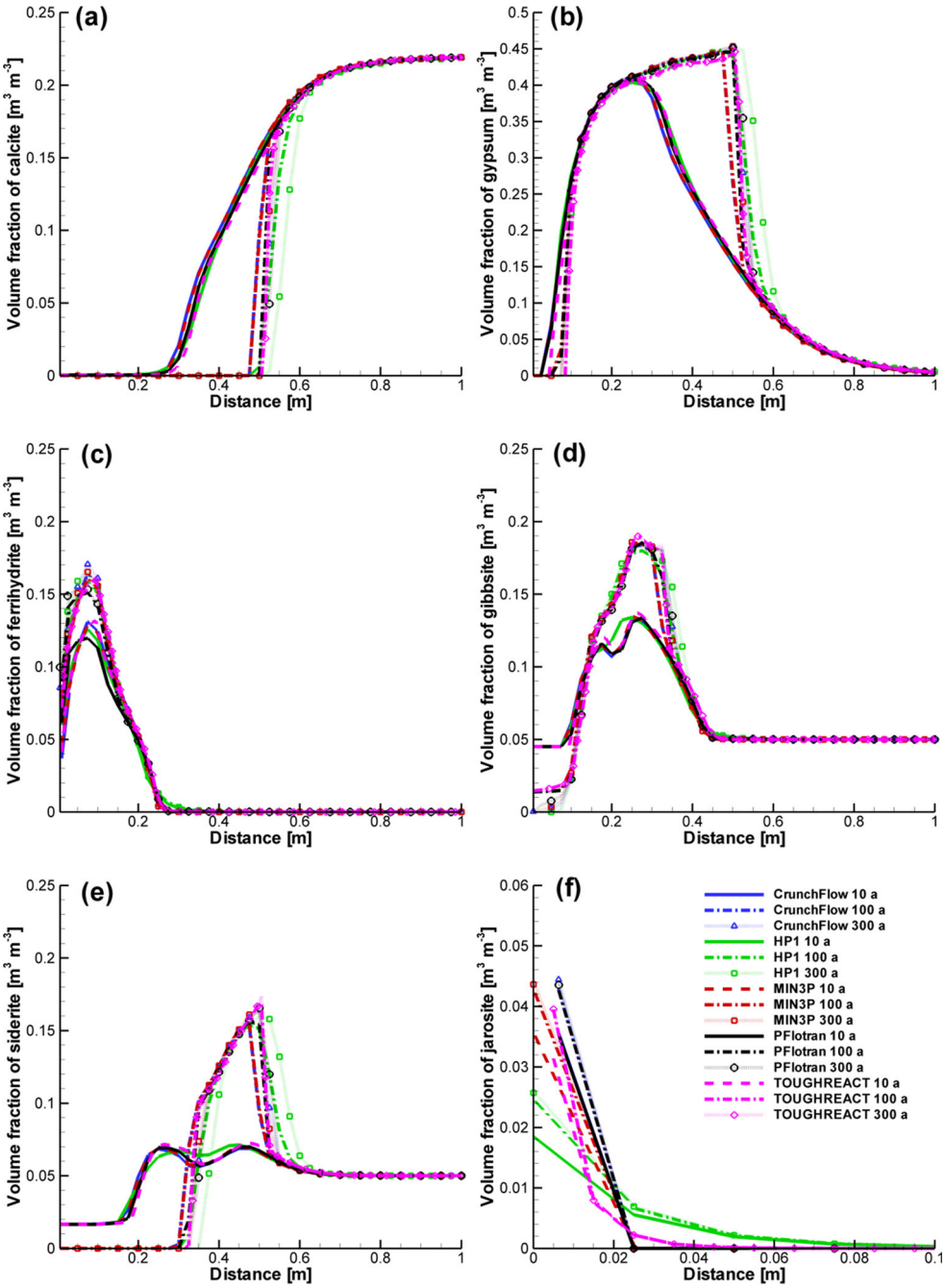

Fig. 9 Comparison of volume fraction profiles (B5) of calcite (**a**), gypsum (**b**), ferrihydrite (**c**), gibbsite (**d**), siderite (**e**) and jarosite (**f**) at 10, 100 and 300 years simulated by CrunchFlow, HP1, MIN3P, PFlotran, and TOUGHREACT

The high porosity zones (in red) formed through the dissolution of calcite and are most prevalent in the regions of higher initial hydraulic conductivity (compare Figs. 12 and 1).

Closer inspection of simulated results shown in Fig. 12 reveal different patterns between the codes for the porosity close to the inlet: porosity fingering near the inlet is similar for MIN3P and CrunchFlow, while a layer of higher porosity formed at the inlet boundary for PFlotran and TOUGHREACT. These differences are due to the slightly different treatment of the boundary conditions and domain discretization by participating codes. MIN3P and CrunchFlow use half-sized cells at the boundary and the nodes are located at the boundary. PFlotran uses fullsized cells at the solution boundary, which results in a slightly different redistribution of flow near the boundary. TOUGHREACT uses special cells at the boundary—thin external layers but with very large volume to fix both hydraulic head and chemical conditions. Similar to the PFlotran results, this approach leads to a slightly different redistribution of flow near the boundary cells. Nevertheless, such influences are limited to the cells near the boundaries and dissipate within the solution domain.

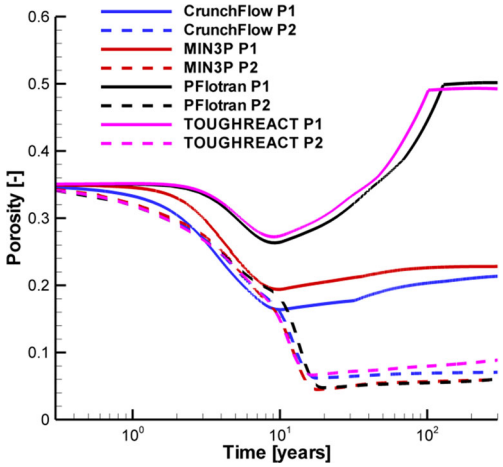

Fig. 10 Comparison of porosity evolution (B6) at observation point P1 (0.1 and 1.0 m) and P2 (0.5 and 1.0 m) simulated by CrunchFlow, MIN3P, PFlotran and TOUGHREACT

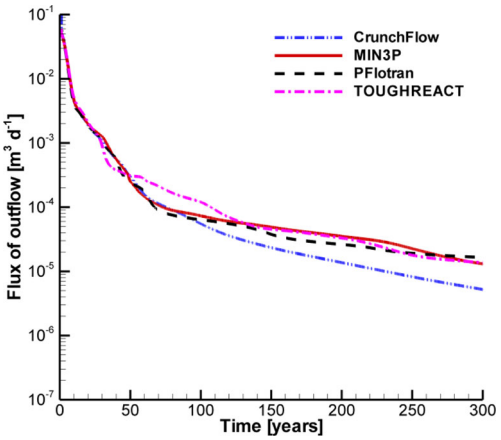

Fig. 11 Comparison of flux evolution at outflow boundary (B6) simulated by CrunchFlow, MIN3P, PFlotran and TOUGHREACT

6 Discussion

We acknowledge that the Carman-Kozeny relationship and Archie's law are not the only relationships to describe the dependency of permeability and tortuosity on porosity. Multiple alternative relationships exist to describe permeability and tortuosity evolution (e.g., [27]). The model comparison presented here showed good agreement between the five codes, but this does not imply that any of the codes—as is—is applicable to simulate permeability or tortuosity evolution at a field site or in a laboratory experiment. It needs to be evaluated whether the implemented relationships are suitable for the site or experimental conditions. However, most of the alternative relationships such as the Brinkmann or Fair-Hatch model for permeability will also be a function of porosity [28] and the general findings of the present investigation should therefore also be relevant for other approaches. Lastly, it has to be recognized that permeability and tortuosity are not only functions of porosity, but may also depend on micro-structural transformations that are taking place, i.e., different secondary minerals may affect permeability in different ways due to their different growth habit [29].

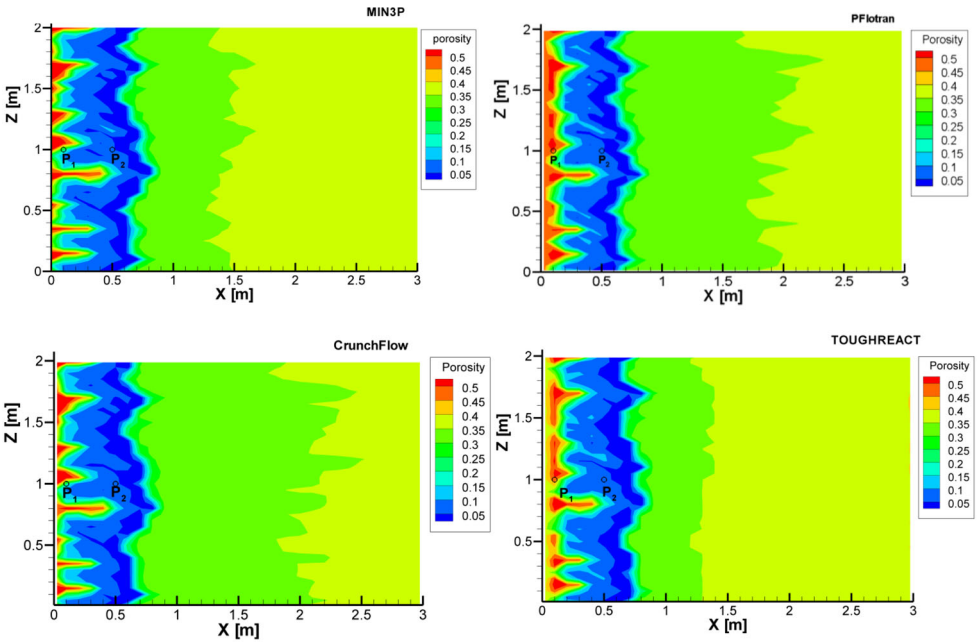

Fig. 12 2D distribution of porosity (B6) simulated by MIN3P, CrunchFlow and PFlotran and TOUGHREACT at 300 years, and the positions of the observation points P1 (x = 0.1 m, z = 1.0 m) and P2 (x = 0.5 m, z = 1.0 m)

7 Conclusions

A sixlevel benchmark problem with increasing complexity for flow, geochemical and mineralogical conditions was analyzed with five different reactive transport codes (i.e. CrunchFlow, HP1, MIN3P, PFlotran and TOUGHREACT) The purpose of the benchmarking exercise was to evaluate the robustness of various numerical implementations of permeability-porosity and tortuosity-porosity relationships to assess the feedback between flow and reactive transport with the potential for local phase disappearance, and the tendency for complete clogging due to mineral precipitation.

Generally speaking, the simulation results appear to be robust and not dependent on the employed code. Simulating porosity enhancement due to mineral dissolution proved to be an easier task than simulating clogging. Increasing complexity due to the inclusion of additional transport mechanisms and a more complex mineralogical assemblage had an impact on the agreement of the model results obtained by the various codes. Although all codes showed good agreement of the predicted mineralogical assemblage and the clogging locations, absolute values of mass fluxes differed substantially. As discussed, these results have to be seen in perspective, considering that the results of all codes agree in the sense that flux reductions are near 100 % for the clogging scenarios. Although differences exist in terms of the absolute flux values, the impact on interpretation of the results would be very limited or even negligible. Nevertheless, these results highlight the difficulties to simulate problems with pore clogging and phase disappearance. Interestingly, the 2D problem (B6) showed better agreement amongst the codes than the equivalent 1D problem (B5), despite the additional complexity in terms of dimensionality and heterogeneity. Although local differences in porosity and mineral assemblage were significant, agreement between overall outflow was good.

This benchmarking exercise also highlights that the implementation of the permeability-porosity and tortuosity-porosity relationships, the activity correction model, and the numerical methods (e.g. spatial weighting schemes) can significantly affect the benchmarking results. A consistent numerical treatment is crucial for the benchmarking of reactive transport codes.

Acknowledgments Financial support for this work was provided by the Nuclear Waste Management Organization (NWMO) and the Natural Sciences and Engineering Research Council of Canada (NSERC) through research grants held by K.U. Mayer. This research was also supported by an internal BRGM research project entitled PMME REP CODSPE2013.

References

1. Wagner, R., Kühn, M., Meyn, V., Pape, H., Vath, U., Clauser, C.: Numerical simulation of pore space clogging in geothermal reservoirs by precipitation of anhydrite. Int. J. Rock Mech. Min. Sci. **42**, 1070–1081 (2005)
2. Annandale, J.G., Jovanovic, N.Z., Benadè, N., Tanner, P.D.: Modelling the long-term effect of irrigation with gypsiferous water on soil and water resources. Agric. Ecosyst. Environ. **76**, 109–119 (1999)
3. Houben, G.J.: Corrigendum to iron oxide incrustations in wells—part 1: Genesis, mineralogy and geochemistry. Appl. Geochem. **18**(6), 927–939 (2003)
4. Rinck-Pfeiffer, S.M., Ragusa, S.R., Sztajnbok, P., Vandevelde, T.: Interrelationships between biological, chemical and physical processes as an analog to clogging in aquifer storage and recovery (ASR) wells. Water Res. **34**(7), 2110–2118 (2000)
5. De Windt, L., Pellegrini, D., van der Lee, J.: Coupled modeling of cement/claystone interactions and radionuclide migration. J. Contam. Hydrol. **68**(3–4), 165–182 (2004)
6. Xie, M., Kolditz, O., Moog, H.C.: A geochemical transport model for thermo-hydro-chemical (THC) coupled processes with saline water. Water Resour. Res. **47**(2), W02545 (2011). doi:10.1029/2010WR009270
7. Liu, S., Jacques, D., Govaerts, J., Wang, L.: Conceptual model analysis of interaction at a concrete–Boom Clay interface. Phys. Chem. Earth (2014). doi:10.1016/j.pce.2013.11.009
8. Lagneau, V., van der Lee, J.: Operator-splitting-based reactive transport models in strong feedback of porosity change: the contribution of analytical solutions for accuracy validation and estimator improvement. J. Contam. Hydrol. **112**, 118–129 (2010)
9. Hayek, M., Kosakowski, G., Churakov, S.: Exact analytical solutions for a diffusion problem coupled with a precipitation-dissolution reaction and feedback of porosity change. Water Resour. Res. (2011). doi:10.1029/2010WR010321
10. Hayek, M., Kosakowski, G., Jakob, A., Churakov, S.: A class of analytical solutions for multidimensional multispecies diffusive transport coupled with precipitation-dissolution reactions and porosity changes. Water Resour. Res. (2012). doi:10.1029/2011WR011663
11. Carrayrou, J., Hoffmann, J., Knabner, P., Kräutle, S., de Dieuleveult, C., Erhel, J., van der Lee, J., Lagneau, V., Mayer, K.U., Macquarrie, K.T.B.: Comparison of numerical methods for simulating strongly nonlinear and heterogeneous reactive transport problems-the MoMaS benchmark case. Comput. Geosci. **14**(3), 483–502 (2010)
12. Allison, J.D., Brown, D.S., Novo-Gradac, K.J.: MINTEQA2/PRODEFA2, a geochemical assessment model for environmental systems: version 3.0 user's manual. United States Environmental Protection Agency, Office of Research and Development, Washington, DC, EPA/600/3-91/021, pp. 106 (1991)
13. Steefel, C.I., Appelo, C.A.J., Arora, B., Jacques, D., Kalbacher, T., Kolditz, O., Lagneau, V., Lichtner, P.C., Mayer, K.U., Meeussen, J.C.L., Molins, S., Moulton, D., Shao, H., Šimůnek, J., Spycher, N., Yabusaki, S.B., Yeh, G.T.: Reactive transport codes for subsurface environmental simulation. Comput. Geosci. (2014). doi:10.1007/s10596-014-9443-x
14. Jacques, D., Šimůnek, J., Mallants, D., van Genuchten, M.T.h.: Modeling Coupled Hydrologic and Chemical Processes: Long-Term Uranium Transport following Phosphorus Fertilization. Vadose Zone J. **7**(2), 698–711 (2008). doi:10.2136/vzj2007.0084

15. Jacques, D., Šimůnek, J., Mallants, D., van Genuchten, M.Th.: Modelling coupled water flow, solute transport and geochemical reactions affection heavy metal migration in a Podzol soil. Geoderma **145**, 449–461 (2008)
16. Mayer, K.U., Frind, E.O., Blowes, D.W.: Multicomponent reactive transport modeling in variably saturated porous media using a generalized formulation for kinetically controlled reactions. Water Resour. Res. (2002). doi:10:1029/2001WR000862
17. Mayer, K.U., MacQuarrie, K.T.B.: Solution of the MoMaS reactive transport benchmark with MIN3P—model formulation and simulation results. Comput. Geosci. (2010). doi:10.1007/s10596-009-9158-6
18. Lichtner, P.C., Hammond, G.E., Lu, C., Karra, S., Bisht, G., Andre, B., Mills, R.T., Kumar, J.: PFLOTRAN User manual: A Massively Parallel Reactive Flow and Transport Model for Describing Surface and Subsurface Processes (2013)
19. Xu, T., Sonnenthal, E.L., Spycher, N., Pruess, K.: TOUGHREACT user's guide: a simulation program for non-isothermal multiphase reactive geochemical transport in variable saturated geologic media. In: Lawrence Berkeley National Laboratory Report LBNL-55460 (Ed.) (2004)
20. Xu, T., Sonnenthal, E., Spycher, N., Pruess, K.: TOUGHREACT—a simulation program for non-isothermal multiphase reactive geochemical transport in variably saturated geologic media: applications to geothermal injectivity and CO_2 geological sequestration. Comput. Geosci. **32**, 145–165 (2006)
21. Xu, T., Spycher, N., Sonnenthal, E., Zhang, G., Zheng, L., Pruess, K.: TOUGHREACT Version 2.0: a simulator for subsurface reactive transport under non-isothermal multiphase flow conditions. Comput. Geosci. **37**, 763–774 (2011)
22. Carrier, W.D.: Goodbye, Hazen; Hello Kozeny-Carman. J. Geotech. Geoenviron. Eng. (2003). doi:10.1061/(ASCE)1090-0241(2003)129:11(1054)
23. Millington, R.J., Quirk, J.P.: Permeability of porous solids. Trans. Faraday Soc. **57**, 1200–1207 (1961)
24. Lichtner, P.C.: In: Lichtner, P.C., Steefel, C.I., Oelkers, E.H. (eds.): Continuum formulation of multicomponent-multiphase reactive transport, vol. 34, pp. 1–81. Mineralogical Society of America, Washington (1996). (Chapter 1)
25. Parkhurst, D.L., Appelo, C.A.J.: User's guide to PHREEQC—a computer program for speciation, batch-reaction, one-dimensional transport, and inverse geochemical calculations. In: Survey, U.S.G. (ed.): Water-resources investigations, Denver (1999)
26. Marty, N.C.M., Tournassat, C., Burnol, A., Giffaut, E., Gaucher, E.C.: Influence of reaction kinetics and mesh refinement on the numerical modelling of concrete/clay interactions. J. Hydrol. **364**(1–2), 58–72 (2009). doi:10.1016/j.jhydrol.2008.10.013
27. Saripalli, K.P., Meyer, P.D., Bacon, D.H., Freedman, V.L.: Changes in hydrologic properties of aquifer media due to chemical reactions: a review. Crit. Rev. Environ. Sci. Technol. **31**(2), 311–349 (2001)
28. Le Gallo, Y., Bildstein, O., Brosse, E.: Coupled reaction-flow modelling of diagenetic changes in reservoir permeability, porosity and mineral compositions. J. Hydrol. **209**, 366–388 (1998)
29. Gouze, P., Coudrain-Ribstein, A.: Chemical reactions and porosity changes during sedimentary diagenesis. Appl. Geochem. **17**, 39–47 (2002)